The crystal structure of α-$PbSnF_4$ and its anion diffusion mechanism

2005 J. Phys.: Condens. Matter 17 845

(http://iopscience.iop.org/0953-8984/17/6/006)

INSTITUTE OF PHYSICS PUBLISHING JOURNAL OF PHYSICS: CONDENSED MATTER

J. Phys.: Condens. Matter **17** (2005) 845–861 doi:10.1088/0953-8984/17/6/006

The crystal structure of α-$PbSnF_4$ and its anion diffusion mechanism

M Castiglione[1], P A Madden[1], P Berastegui[2] and S Hull[3,4]

[1] Chemistry Department, Oxford University, South Parks Road, Oxford OX1 3QZ, UK
[2] Department of Inorganic Chemistry, Arrhenius Laboratory, Stockholm University, S-106 91 Stockholm, Sweden
[3] The ISIS Facility, Rutherford Appleton Laboratory, Chilton, Didcot, Oxfordshire OX11 0QX, UK

E-mail: s.hull@rl.ac.uk

Received 4 November 2004, in final form 10 January 2005
Published 28 January 2005
Online at stacks.iop.org/JPhysCM/17/845

Abstract

The crystal structure of $PbSnF_4$ and the nature of the anion diffusion mechanism which characterizes its high ionic conductivity have been investigated by impedance spectroscopy, powder neutron diffraction and computer simulation methods. The ionic conductivity of $PbSnF_4$ undergoes small, but abrupt, increases at 608(4) and 672(3) K characteristic of the $\alpha \rightarrow \beta$ and $\beta \rightarrow \gamma$ phase transitions. The ambient temperature α-$PbSnF_4$ phase possesses a tetragonal crystal structure (space group $P4/nmm$), derived from the cubic fluorite arrangement by ordering of the cations in the scheme PbPbSnSnPbPb$\cdots$ along the [001] direction. However, the Sn^{2+}–Sn^{2+} layers contain essentially no F^-, with the displaced anions residing in the Pb^{2+}–Sn^{2+} layers and showing significant disorder, particularly at temperatures close to the upper limit of stability of the α phase. Computer simulations, using interionic potentials derived from first-principles calculations and containing realistic representations of polarization effects, are in good agreement with the measured ionic conductivity and successfully reproduce the experimentally determined ionic distribution. Analysis of the simulated ionic motions demonstrate that the impressive ionic conductivity of α-$PbSnF_4$ at temperatures close to ambient is a consequence of anion diffusion within the Pb^{2+}–Sn^{2+} layers, whilst those F^- within the Pb^{2+}–Pb^{2+} layers are immobile. At temperatures close to the melting point of the simulated system, increased transfer of anions between the various Pb^{2+}–Pb^{2+}, Pb^{2+}–Sn^{2+}, Sn^{2+}–Sn^{2+} layers is observed, as the system tends towards a more isotropic anion diffusion process.

(Some figures in this article are in colour only in the electronic version)

[4] Author to whom any correspondence should be addressed.

1. Introduction

Halide compounds of stoichiometry MX_2 which possess the cubic fluorite crystal structure (space group $Fm\bar{3}m$) have been extensively studied owing to their high-temperature superionic properties [1–3]. This behaviour is characterized by a rapid, though continuous, increase in the ionic conductivity of compounds such as CaF_2, BaF_2, $SrCl_2$ and β-PbF_2 on heating, due to the development of extensive, dynamic Frenkel disorder within the anion sublattice [4]. The superionic transition is also associated with anomalous lattice expansion [5] and a peak in the specific heat C_p, whose maximum is generally taken to define the superionic transition temperature T_c [6]. Typically, T_c is observed to be $\sim 0.8T_m$ (where T_m is the melting temperature in kelvin), though β-PbF_2 has a significantly lower value of $T_c = 711$ K $\approx 0.61T_m$ [6]. This observation has been attributed to increased cation polarization effects associated with the Pb^{2+} ion, which effectively increase the relative stability of more distorted local anion environments which occur during the diffusion process [7].

It has been widely demonstrated that the ionic conductivity of fluorite structured compounds such as β-PbF_2 can be enhanced at temperatures well below T_c by the addition of aliovalent cations, due to the formation of charge compensating vacancies or interstitials within the anion sublattice (see, for example, [8, 9]). By contrast, the addition of isovalent cations such as Sn^{2+} to β-PbF_2 does not change the overall stoichiometry. Intuitively, since the dopant Sn^{2+} is smaller than the host Pb^{2+}, both the unit cell volume and the ionic conductivity of $Pb_{1-x}Sn_xF_2$ would be expected to decrease with x [10]. However, both have been experimentally observed to increase with x [11–13], at least up to the fluorite solid solution limit at $x \approx 0.20$–0.25, and a number of complex superstructures are observed at higher dopant levels [14]. These observations have been attributed to the greater stereoactivity of the $5s^2$ lone-pair of the Sn^{2+} ions, which favour long-range ordering of the two cation species and have also been suggested to play an important role in stabilizing the structure of the $x = 0.5$ phase, $PbSnF_4$ [14, 15].

The synthesis of lead(II) tetrafluorostannate(II), $PbSnF_4$, was first reported in 1967 [16] and the compound has subsequently been shown to possess one of the highest values of ionic conductivity of any fluorine ion conductor at temperatures close to ambient ($\sigma \sim 10^{-1}\ \Omega^{-1}\ cm^{-1}$ at $\sim$470 K [17]). As a consequence, $PbSnF_4$ has been considered for use as a negative electrode for Li-ion batteries [18] and within fast response oxygen gas sensors [19].

$PbSnF_4$ adopts the cubic fluorite structure (space group $Fm\bar{3}m$) in its high-temperature γ phase, which is stable within a narrow (approximately 30 K) range immediately below its melting point of 693 K [17, 20]. The Pb^{2+} and Sn^{2+} are randomly distributed over the available cation sites in the γ-$PbSnF_4$ phase so that, on average, it is isostructural with β-PbF_2. At lower temperatures a number of different phases are formed, depending on the cooling rate [17, 20, 21]. Investigations of the crystal structure of $PbSnF_4$ at ambient temperature are made difficult by the formation of a number of closely related phases with monoclinic [15, 21], orthorhombic [17, 22–24] and tetragonal [16, 20, 23, 25–29] symmetries, depending on the preparation method [30]. However, their structures are all fluorite-related and generally contain long-range ordering of the cations with PbPbSnSnPbPb$\cdots$ layers perpendicular to one of the pseudo-cubic axes. The most widely studied form is the α phase of $PbSnF_4$ prepared by solid state synthesis of the constituent binary fluorides. Its unit cell is tetragonal, with lattice parameters related to those of the parent fluorite structure by $a_\alpha = a_F/\sqrt{2}$ and $c_\alpha = 2 \times a_F$. Whilst the symmetry has generally been agreed to be $P4/nmm$, a number of different reports concerning the distribution of anions within the various Pb^{2+}–Pb^{2+}, Pb^{2+}–Sn^{2+} and Sn^{2+}–Sn^{2+} layers perpendicular to the [001] direction have been published [20, 23, 25–29].

In this paper we report the results of an impedance spectroscopy investigation of the temperature dependence of the ionic conductivity of $PbSnF_4$ and a powder neutron diffraction

study of the crystal structure of the tetragonal α-$PbSnF_4$ phase at temperatures close to ambient. These data are used to validate computer simulations, which in turn provide an insight into the F^- diffusion mechanism which characterizes the high ionic conductivity observed at relatively modest temperatures. Finally, the structural properties of $PbSnF_4$ will be discussed, with emphasis on the role of highly polarizable cations (as opposed to lone-pair electrons) in promoting extensive anion disorder.

2. Experimental details

A sample of α-$PbSnF_4$ was prepared by mixing stoichiometric amounts of the previously dried α-PbF_2 and SnF_2 in an argon-filled dry box. The mixture was then pelletized and sintered in a gold tube under dynamic vacuum at 473 K overnight. The powder was then reground, pelletized, sintered for a further 24 h at 548 K and subsequently annealed at 473 K for 48 h in flowing argon.

Two terminal measurements of the ionic conductivity were performed using a pelleted sample of 6 mm diameter and 6 mm length. This was held between two spring loaded platinum discs inside a boron nitride cell which is inserted into the hotzone of a horizontal tube furnace. Details of this device can be obtained elsewhere [31]. Complex impedance measurements were performed approximately every 3 min whilst the furnace temperature was ramped up then down at 60 K h^{-1}. The maximum temperature used was 694 K. A Solartron S1260 frequency response analyser determined the conventional Z–Z′ Bode plot over the frequency range from 0.1 Hz to 10 MHz. The real component of the sample impedance Z_S was determined using the program IMMFIT [31]. All measurements were performed under dynamic vacuum of $\sim 10^{-2}$ Pa and temperature monitoring obtained using chromel–alumel thermocouples located $\sim$2 mm from the sample pellet.

The neutron diffraction experiments were performed on the Polaris powder diffractometer at the ISIS facility, UK [32], with the sample encapsulated inside a thin-walled vanadium can of $\sim$11 mm diameter and $\sim$40 mm height. Diffraction data were collected using the backscattering detector bank which covers the scattering angles $135^\circ < \pm 2\theta < 160^\circ$ and provides data over the d-spacing range $0.5 < d(\text{Å}) < 3.2$ with an essentially constant resolution of $\Delta d/d \sim 5 \times 10^{-3}$. Approximately 2 h was required to collect diffraction data of sufficient statistical accuracy to determine the anion distributions with the α phase of $PbSnF_4$, with data collected at 10 temperatures in the range $298(3)\ \text{K} \leqslant T \leqslant 610(2)\ \text{K}$.

The time-averaged distributions of the mobile anions within the unit cell of α-$PbSnF_4$ were determined using a maximum entropy analysis of the powder neutron diffraction data based on the MemSys package (Maximum Entropy Data Consultants Ltd, Cambridge, UK) (for details, see [33]). The ability of this technique to probe the densities of mobile ions within ionically conducting phases has recently been demonstrated for the Ag^+ conductors $RbAg_4I_5$ [34] and Ag_2S [35]. Subsequent least-squares profile refinements of the diffraction data were performed using the program TF12LS [36], which is based on the Cambridge Crystallographic Subroutine Library [37].

The quality of the fits was assessed using the usual goodness-of-fit χ^2 statistic, defined by

$$\chi^2 = \sum_{N_D} \frac{(I_{obs} - I_{calc})^2}{(\sigma I_{obs})^2} \Big/ (N_D - N_V),$$

where N_D is the number of data points used in the fit and N_V is the number of fitted variables. I_{obs} and I_{calc} are the observed and calculated intensities, respectively, and σI_{obs} is the estimated standard deviation on I_{obs}, derived from the counting statistics.

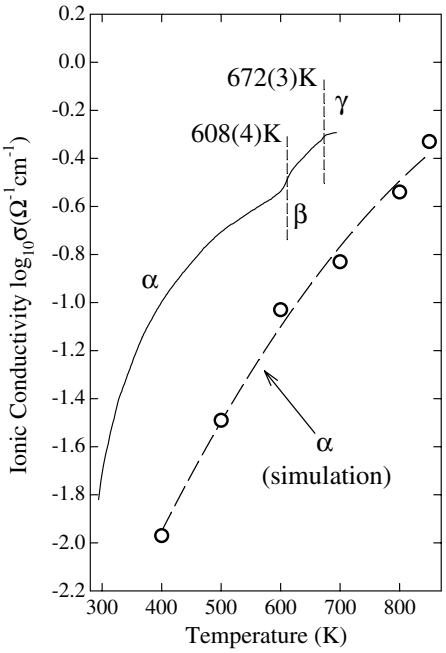

Figure 1. The temperature variation of the measured ionic conductivity σ of $PbSnF_4$ (solid curve), showing the $\alpha \rightarrow \beta$ and $\beta \rightarrow \gamma$ transitions observed at 608(4) and 672(3) K, respectively. The open symbols (O) represent the values obtained from the computer simulations of α-$PbSnF_4$. The dashed curve is a guide to the eye for the latter.

3. Experimental results

3.1. Ionic conductivity measurements

The temperature dependence of the ionic conductivity of $PbSnF_4$ is illustrated in figure 1. The measured value at ambient temperature ($\sigma = 1.2 \times 10^{-2}\ \Omega^{-1}\ \mathrm{cm}^{-1}$) is in good agreement with that published previously [17]. Abrupt changes in the slope of σ versus T are observed at temperatures of 608(4) and 672(3) K. With reference to the work of Pannetier *et al* [20], these can be attributed to the $\alpha \rightarrow \beta$ and $\beta \rightarrow \gamma$ phase transitions, respectively, though the former occurs at a somewhat higher temperature in this study. There is no evidence of a transition at a temperature ~350 K reported in some other studies [17, 21, 24]. In the context of this paper, the data presented in figure 1 are primarily used to validate the results of computer simulation studies of the α phase of $PbSnF_4$, and no further discussion of the β and γ phases will be presented here.

3.2. Neutron diffraction measurements

The measured d-spacings of the Bragg peaks observed from α-$PbSnF_4$ at ambient temperature can be indexed on the basis of a tetragonal unit cell with lattice parameters $a \approx 4.232$ Å and $c \approx 11.426$ Å. Since the hkl values for absent reflections are consistent with $P4/nmm$ symmetry it is reasonable to assume that this phase corresponds to the α form described previously [16, 20, 23, 25–29].

Earlier studies of the crystal structure of α-$PbSnF_4$ using x-ray and neutron diffraction techniques have concluded that the two cation species form planes perpendicular to the [001]

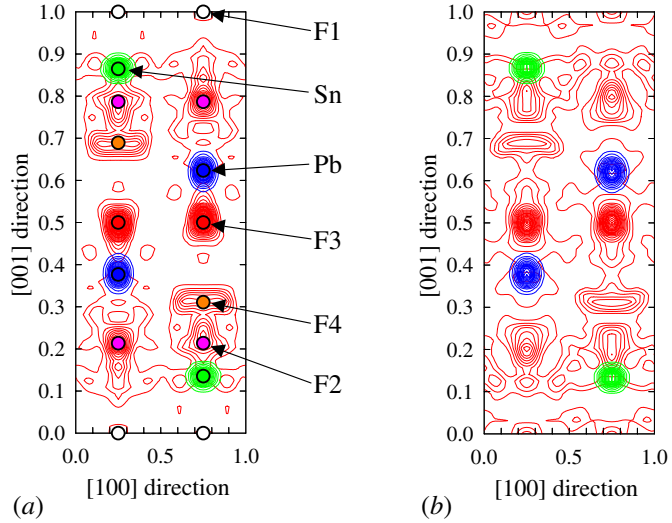

Figure 2. An (010) projection showing the experimentally determined time-averaged distribution of ions within α-$PbSnF_4$ at (*a*) 298(3) K and (*b*) 572(2) K. The contours show the Pb^{2+}, Sn^{2+} and F^- densities, with the locations of the various Pb, Sn and F1–F4 sites determined from the least-squares refinements of the data illustrated in (*a*). The increased anion disorder within the Pb^{2+}–Sn^{2+} layers and the presence of some F^- on the F1 sites at higher temperatures is apparent in (*b*).

direction with an ordering scheme PbPbSnSnPbPb$\cdots$[16, 20, 25–29]. In relation to the fluorite-structured parent arrangement, the equivalent anion positions within the Sn^{2+}–Sn^{2+}, Pb^{2+}–Sn^{2+} and Pb^{2+}–Pb^{2+} layers of α-$PbSnF_4$ are in the 2(a) positions at 3/4, 1/4, 0 and 1/4, 3/4, 0, the 4(f) positions at 3/4, 1/4, z, 1/4, 3/4, z, 3/4, 1/4, $\bar{z}$ and 1/4, 3/4, $\bar{z}$ with $z = 1/4$, and the 2(b) positions at 3/4, 1/4, 1/2 and 1/4, 3/4, 1/2, respectively. Following the notation used in previous studies, these positions are labelled F1, F2 and F3, respectively [26, 28]. However, there are significant differences between the anion distribution determined by the previous diffraction studies of α-$PbSnF_4$ [20, 25–29], with between three and five sites employed, many of which are only partially occupied, and considerable debate concerning the extent to which F^- populate the F1 sites within the Sn^{2+}–Sn^{2+} layers.

Attempts to fit the neutron diffraction data collected during this study using the various reported structural models [20, 25–29] gave moderate success, but significant differences between the measured and fitted profiles suggested that the anion distribution was not correctly modelled. As a consequence, our initial analysis of the data collected from α-$PbSnF_4$ at 298(3) K adopted a more general approach. The cations were assumed to form ordered double layers of the type described above and maximum entropy difference Fourier maps were used to investigate the anion distribution. The resultant reconstructed time-averaged density of ions within the unit cell is illustrated in figure 2(*a*).

It is clear from figure 2(*a*) that there is no significant occupancy of the F1 sites and the Sn^{2+}–Sn^{2+} layers are essentially empty. This contrasts with the findings of some previous reports [27, 29]. However, the F3 sites within the Pb^{2+}–Pb^{2+} layers are well defined and centred at the fluorite-equivalent positions, whilst the anion distribution within the Pb^{2+}–Sn^{2+} layers is rather disordered. This feature is likely to contribute to the high ionic conductivity observed for α-$PbSnF_4$ at ambient temperature (figure 1) and also explains the lack of agreement between previous diffraction studies. Close inspection of the three-dimensional anion distribution

Table 1. Temperature dependence of the lattice parameters (a and c) and the positional parameters (z_{Pb}, z_{Sn}, z_{F2} and z_{F4}) of α-$PbSnF_4$ obtained by least-squares refinements of the powder neutron diffraction data. The Pb^{2+} and Sn^{2+} are located in the 2(c) positions of space group $P4/nmm$ at 1/4, 1/4, z and 3/4, 3/4, $\bar{z}$ and the locations of the various F sites are described in the text.

	Lattice parameters		Positional parameters			
T (K)	a (Å)	c (Å)	z_{Pb}	z_{Sn}	z_{F2}	z_{F4}
298(3)	4.231 38(2)	11.426 29(8)	0.3772(3)	0.8669(3)	0.2167(7)	0.6864(7)
367(2)	4.242 68(3)	11.440 59(14)	0.3770(3)	0.8662(4)	0.2137(8)	0.6868(8)
430(2)	4.250 58(3)	11.452 14(14)	0.3769(3)	0.8660(4)	0.2142(8)	0.6875(8)
476(2)	4.258 14(3)	11.466 16(14)	0.3770(3)	0.8658(4)	0.2129(8)	0.6888(9)
508(2)	4.263 98(3)	11.477 95(16)	0.3774(3)	0.8659(4)	0.2134(8)	0.6893(10)
530(2)	4.267 75(3)	11.487 39(16)	0.3770(3)	0.8662(4)	0.2130(8)	0.6888(10)
551(2)	4.271 53(3)	11.498 73(17)	0.3773(3)	0.8663(5)	0.2125(8)	0.6884(11)
572(2)	4.275 39(3)	11.513 61(18)	0.3768(4)	0.8674(5)	0.2138(9)	0.6893(14)
591(2)	4.278 70(4)	11.542 2(2)	0.3763(6)	0.8669(7)	0.2125(12)	0.6880(15)

within the unit cell (figure 2(a)) indicates that, to a good approximation, the time-averaged F^- positions within the Pb^{2+}–Sn^{2+} layers can be modelled using the F2 sites (though slightly relaxed in the [001] direction towards the Sn^{2+}–Sn^{2+} layers) and allowing the anions displaced from the F1 sites to occupy 2(c) sites at 1/4, 1/4, z and 3/4, 3/4, $\bar{z}$ with $z \sim 0.7$. The latter are labelled F4. Least-squares refinements of the diffraction data using this starting model converged rapidly and provided a good fit to the data, provided that the thermal parameters of the ions, and in particular the F2 and F4 anions, were allowed to vary anisotropically. The fitted parameters comprised a scale parameter, 15 coefficients of a polynomial describing the background scattering, two lattice parameters, four positional parameters, 11 anisotropic thermal vibration parameters and three peakshape parameters. The values of the final fitted parameters are listed in tables 1 and 2 and the structural model is illustrated in figure 3. The quality of the final fit is shown in figure 4. Whilst some residual differences between the measured and calculated profiles remain, these are largely a consequence of a small unidentified impurity phase within the sample and a slight hkl dependence of the peak widths of α-$PbSnF_4$. Nevertheless, the reliability of the structural model is confirmed by the similarity between the goodness-of-fit parameter obtained using this approach[5] ($\chi^2 = 3.24$) and that provided by a model-independent fit ($\chi^2 = 2.93$). The latter treats the intensities of all the allowed reflections as variables (plus the lattice parameters and background coefficients) and thus provides a 'best' value of χ^2 that can be obtained when adopting a structural model.

The structural description determined at 298(3) K was used as the starting model for the least-squares refinement of the diffraction data collected at the first high temperature (367(2) K) and this iterative procedure was followed to analyse the data collected at nine temperatures up to 572(2) K. Data collected at the next temperature of 610(2) K contained additional small peaks. These may be assigned to the appearance of the β phase of $PbSnF_4$, and is consistent with the temperature of the $\alpha \rightarrow \beta$ transition (608(4) K) observed within the ionic conductivity data (figure 1).

Least-squares refinements of the diffraction data collected at temperatures near to the upper limit of the stability of the α phase of $PbSnF_4$ showed slightly poorer fits than those obtained at

[5] The number of data points (N_D), fitted variables (N_V) and Bragg peaks (N_P) used in the final least-squares fit were 3693, 36 and 634, respectively. The profile (R_P), weighted profile (R_{WP}) and expected (R_{EXP}) R-factors were 2.15%, 1.48% and 0.82%, respectively, and are given by $R_P^2 = \sum_{N_D}(I_{obs} - I_{calc})^2 / \sum_{N_D}(I_{obs})^2$, $R_{WP}^2 = \sum_{N_D} \frac{(I_{obs}-I_{calc})^2}{(\sigma I_{obs})^2} / \sum_{N_D} \frac{(I_{obs})^2}{(\sigma I_{obs})^2}$ and $R_{EXP}^2 = (N_D - N_V) / \sum_{N_D} \frac{(I_{obs})^2}{(\sigma I_{obs})^2}$ [38].

Table 2. Temperature dependence of the anisotropic thermal vibration parameters B_{ij} of α-$PbSnF_4$ obtained by least-squares refinements of the powder neutron diffraction data. The B_{ij} are the components of the anisotropic thermal vibrations, defined by $B_{ij} = 8\pi^2\langle u_{ij}^2\rangle$, where u_{ij} is the mean-squared amplitude of the vibration in direction ij.

	Pb		Sn		F2			F3		F4	
T (K)	B_{11} (Å^2)	B_{33} (Å^2)	B_{11} (Å^2)	B_{33} (Å^2)	B_{11} (Å^2)	B_{22} (Å^2)	B_{33} (Å^2)	B_{11} (Å^2)	B_{33} (Å^2)	B_{11} (Å^2)	B_{33} (Å^2)
298(3)	1.47(5)	2.96(10)	1.90(7)	0.96(13)	24.9(8)	3.1(2)	23.4(9)	1.37(6)	3.35(15)	25.9(7)	4.0(4)
367(2)	1.61(5)	3.57(11)	2.23(8)	1.27(14)	24.6(9)	4.2(3)	23.9(9)	1.70(7)	4.02(18)	26.6(8)	5.2(5)
430(2)	1.82(5)	3.95(12)	2.37(8)	1.51(15)	25.5(9)	4.7(3)	24.8(9)	1.86(7)	4.19(19)	26.2(8)	5.6(5)
476(2)	1.96(6)	4.26(13)	2.58(9)	1.80(17)	26.3(9)	5.2(3)	23.6(9)	2.07(8)	4.6(2)	27.0(8)	7.4(6)
508(2)	2.11(6)	4.41(14)	2.64(9)	2.08(18)	26.2(9)	5.1(3)	23.3(9)	2.21(8)	4.7(2)	27.7(9)	9.2(7)
530(2)	2.27(6)	4.65(15)	2.78(10)	2.19(19)	29.7(10)	4.7(3)	24.7(10)	2.38(9)	4.8(2)	27.6(9)	8.9(7)
551(2)	2.39(7)	4.81(16)	2.79(10)	2.3(2)	28.8(10)	5.1(3)	24.7(10)	2.57(9)	4.7(2)	29.9(10)	9.9(8)
572(2)	2.50(8)	5.62(19)	2.89(11)	2.1(2)	31.7(12)	4.8(3)	28.2(13)	2.64(10)	5.2(3)	29.4(11)	12.8(11)
591(2)	2.59(9)	5.3(3)	3.26(13)	2.3(2)	33.3(17)	5.9(3)	31(2)	2.87(14)	6.2(4)	32.1(14)	15.0(15)

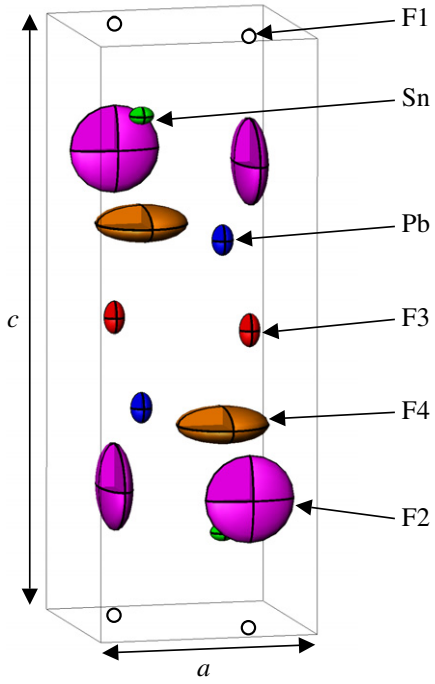

Figure 3. The crystal structure of α-$PbSnF_4$ determined by least-squares refinement of the powder neutron diffraction data collected at 298(3) K. The highly anisotropic thermal vibrations of the anions located at the F2 and F4 positions is clearly visible.

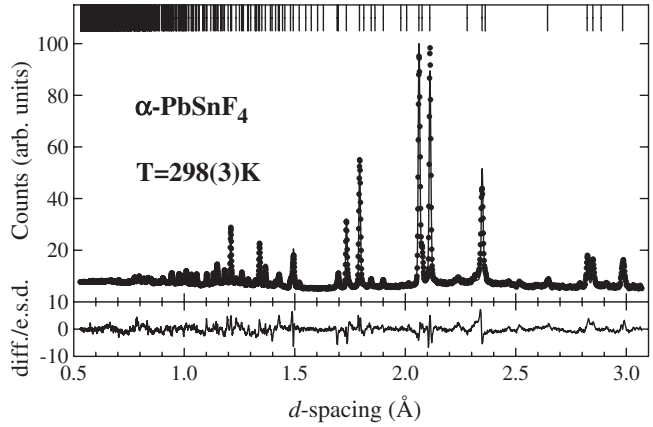

Figure 4. The least-squares fit to the powder neutron diffraction data collected from α-$PbSnF_4$ at 298(3) K. The dots are the experimental data points and the solid line is the calculated profile using the parameters listed in tables 1 and 2. The lower trace shows the difference (measured minus calculated) divided by the estimated standard deviation on the experimental data points. The tick marks along the top of the figure denote the calculated positions of all the Bragg reflections allowed by $P4/nmm$ symmetry.

temperatures close to ambient. A repeat of the maximum entropy difference Fourier procedure using the diffraction data collected at 572(2) K was performed. As illustrated in figure 2(*b*),

there appears to be an increased anion density linking the various F2 and F4 sites within the Pb^{2+}–Sn^{2+} layers, indicative of increased disorder within this plane. Clearly, attempts to model this distribution using only the fully occupied sites illustrated in figure 3 contribute to the slightly poorer quality of the fits to the higher temperature data. However, attempts to provide an unambiguous description of the F^- density using additional partially occupied sites (including those structural models proposed previously [20, 23, 25–29]) were not successful, owing to excessive correlations between the various anisotropic thermal vibration and site occupancy parameters. In addition, figure 2(*b*) shows some evidence of F^- density at the F1 sites within the Sn^{2+}–Sn^{2+} layers, with an upper limit on the anion population of these sites being $\sim$0.2 of the total of $8 \times F^-$ within the unit cell of α-$PbSnF_4$.

4. Computer simulations

4.1. Interaction potentials and simulation details

Molecular dynamics computer simulations of the α phase of $PbSnF_4$ were carried out using ionic interaction potentials, with formal charges, which are derived from those used in previous studies of PbF_2 [7, 39, 40]. Overall, these potentials reproduced the phenomenology of PbF_2 well, except that the transition temperature T_c (position of the heat capacity maximum) was 925 K, rather than 711 K, so that the simulation temperature had to be scaled to compare simulation and experimental data. A crucial aspect of these interaction potentials is the incorporation of the dipole polarization of the anions and cations. Both Pb^{2+} and Sn^{2+} have outer electron configurations involving two electrons in the valence s orbital, i.e. ns^2. Consequently, both have very large dipole polarizabilities [41, 42] (2.5 Å^3 for Pb^{2+}, 2.2 Å^3 for Sn^{2+}, compared to 0.9 Å^3 for an in-crystal F^- ion) because of the low-energy, dipole-allowed intra-valence transition to the ns^1p^1 configuration. Ionic polarization promotes the occupation of low-symmetry sites [43] so that, for example, the adoption of the layered litharge structure by SnO and PbO can be regarded as a consequence of the cation polarization [42].

The interaction potentials consist of pair potentials to describe the short-range repulsion, dispersion and charge–charge interaction:

$$V_{ij}(r_{ij}) = \frac{B_{ij}^{-a_{ij}r_{ij}}}{r_{ij}} + B'_{ij}\mathrm{e}^{-a'_{ij}r_{ij}^2} + \frac{Z_iZ_je^2}{r_{ij}} - \sum_{n=6,8}\frac{C_{n,ij}}{r_{ij}^n}f_{ij}^n.$$

These potentials are of the same form as those used in the PbF_2 work [7]. They differ from the standard Born–Mayer form by use of a steeper repulsive potential than the normal exponential, and by the inclusion of a dispersion damping [44] factor. The parameters to describe the additional Sn^{2+}–Sn^{2+} and Sn^{2+}–F^- interactions were obtained by first calculating appropriate values for the dispersion coefficients (C_6 and C_8) by scaling the Pb^{2+}–Pb^{2+} and Pb^{2+}–F^- values for the changed value of the cation polarizability according to the Starkschall–Gordon expression [41]. The remaining short-range parameters were obtained by modifying the corresponding terms in the PbF_2 potential so that its minimum energy occurred at the experimental crystal structure for SnF_2 [45], whilst keeping the same F^-–F^- interactions and including the polarization potential described below. Finally, the Pb^{2+}–Sn^{2+} terms were obtained by setting the parameters equal to the mean of the values in the Pb^{2+}–Pb^{2+} and Sn^{2+}–Sn^{2+} potentials; in practice, this term does not play a strong role in the results described below in section 4.2. A full set of parameters for the pair potentials is given in table 3.

The polarization effects are treated by methods described at length elsewhere [43]. The requisite parameters are the dipole polarizabilities, α, for each ion, and a set of 'induction-damping' parameters, b_{ij} and c_{ij}, to describe the induction of a dipole on an ion by short-

Table 3. The potential parameters for the Pb^{2+}–Pb^{2+}, Pb^{2+}–Sn^{2+}, Pb^{2+}–F^-, Sn^{2+}–Sn^{2+}, Sn^{2+}–F^- and F^-–F^- interactions used in the computer simulations of α-$PbSnF_4$. The parameters are given in atomic units.

Parameter	Pb^{2+}–Pb^{2+}	Pb^{2+}–Sn^{2+}	Pb^{2+}–F^-	Sn^{2+}–Sn^{2+}	Sn^{2+}–F^-	F^-–F^-
a	2.145	2.1447	1.435	2.145	1.435	2.788
B	4613.6	3336.0	110.3	2412.2	88.8	2576.0
a'	0.0	0.0	1.0	0.0	1.0	0.0
B'	0.0	0.0	50 000.0	0.0	30 000.0	0.0
C_6	111.9	103.6	53.0	96.2	48.8	44.4
C_8	1022.8	930.8	711.0	848.4	654.0	538.8

Table 4. The induction damping parameters for the Pb^{2+}–F^-, Sn^{2+}–F^-, F^-–Pb^{2+} and F^-–Sn^{2+} interactions used in the computer simulations of α-$PbSnF_4$. The parameters are given in atomic units.

Parameter	Pb^{2+}–F^-	Sn^{2+}–F^-	F^-–Pb^{2+}	F^-–Sn^{2+}
b_{ij}	1.8	1.86	1.8	1.86
c_{ij}	−0.3	−0.3	1.0	1.0

range, overlap interaction with its neighbours (in addition to the interionic electric field-induced dipole). The range of this effect is controlled by b_{ij}, and its amplitude by c_{ij}, via the expression [43]

$$f_{ij}(r) = 1 - c_{ij}\left(\sum_{k=0}^{4}\frac{(b_{ij}r)^k}{k!}\right)\mathrm{e}^{-b_{ij}r}.$$

The new b_{ij} values are obtained by scaling the PbF_2 values to allow for the change in cation size, and the same values are used for c_{ij} as in PbF_2. These values are given in table 4.

In the computer simulations, Ewald summations were used to describe all the long-ranged interactions involving charges and dipoles. The integration method [46] allows for simulation in an *NPT* (constant particle number, pressure and temperature) ensemble, where the simulation unit cell shape and size is allowed to change so that the average pressure is isotropic, or in an *NVT* (constant particle number, volume and temperature) ensemble, with fixed periodic boundary conditions. 576 ions were used in the simulations of the α-$PbSnF_4$ phase, and the initial configuration was based on a $4 \times 4 \times 3$ arrangement of 12-atom fluorite unit cells ($a \times a \times 2\sqrt{2}a$), with the Pb^{2+} and Sn^{2+} ions arranged to form layers perpendicular to the c-direction. A long (0.5 ns) simulation in the *NPT* ensemble, at zero pressure and a temperature of 600 K was then undertaken, in order to allow the fluoride ion positions and the cell shape to relax. No exchange of cations was observed at this temperature. At a temperature of 500 K the unit cell volume per formula unit (V/Z) was 106.2 $Å^3$, in good agreement with the value of 103.4 $Å^3$ determined by the powder neutron diffraction studies at 508(2) K (table 1). The unit cell remained tetragonal on average, with the extent of the tetragonal distortion (expressed as $c/2\sqrt{2}a$) being 0.877. Whilst the agreement with the experimental value ($\approx$0.951 at comparable temperatures) is more modest, both indicate a significant compression of the structure along the c-axis relative to the idealized cubic fluorite case.

The configuration obtained at 600 K was then used as the starting point for subsequent calculations. Each simulation at a new temperature was begun with a 45 ps equilibration run in the *NPT* ensemble, with a starting configuration taken from a previous simulation. The production runs were then done in the *NVT* ensemble, using the final cell shape from the equilibration step. The production runs were typically of 45 ps duration.

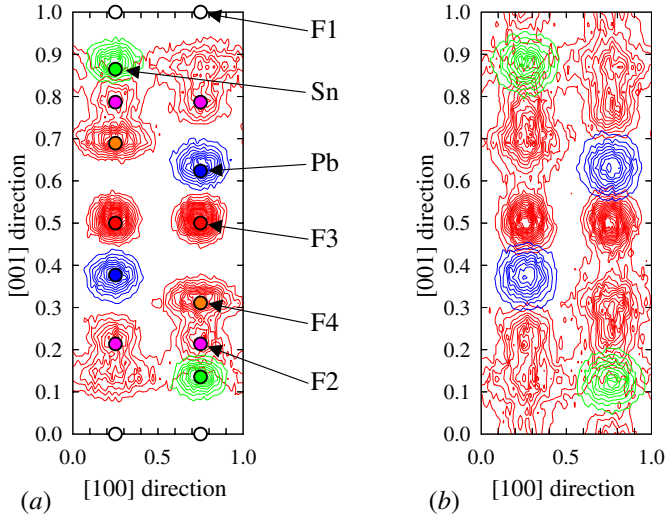

Figure 5. An (010) projection showing the time-averaged distribution of ions within the computer simulations of α-$PbSnF_4$ at (*a*) 700 K and (*b*) 800 K. The contours show the Pb^{2+}, Sn^{2+} and F^- densities, with the locations of the various Pb, Sn and F1–F4 sites determined from the least-squares refinements of the data illustrated in (*a*). The anion disorder within the Pb^{2+}–Sn^{2+} layers is apparent in (*a*), whilst the presence of some F^- on the F1 sites is observed in (*b*).

4.2. Simulation results

Values for the diffusion coefficients of the ions and for the ionic conductivity of α-$PbSnF_4$ were obtained from the long-time slopes of plots of the mean-squared displacement of the ions and of the mean-squared displacement of the charge versus time, as in the PbF_2 calculations [39, 40]. The simulated model for α-$PbSnF_4$ was observed (from the finite values of the diffusion coefficients of the cations) to melt in the *NPT* simulations at a temperature slightly in excess of 850 K. This is higher than the experimental value of ∼693 K [20] though a direct comparison is difficult because, on heating, the α form undergoes structural transitions prior to melting.

The conductivity values determined from the simulations are shown in figure 1, for comparison with the experimental data. It can be seen that the simulated conductivities span the range of the experimental data and would agree rather well with them over a broad temperature range if, in the manner of the PbF_2 work [40], the simulation temperature was scaled down by a factor of about 700/850, which is the ratio of experimental to simulation melting temperatures. The scaling is an attempt to compensate for shortcomings in the interaction potential, which, as described above, was not refined to agree with any of the properties of $PbSnF_4$.

The time-averaged ion densities from the simulation at 700 K are shown in figure 5(*a*). The data are plotted in the same manner as figure 2 for comparison. As discussed above, the simulation temperature of 700 K is comparable to an experimental temperature of ∼580 K and the F^- ion distribution is in good qualitative agreement with the experimental data shown in figure 2(*a*). At this temperature, no F^- ions are found in the F1 sites between the layers of Sn^{2+} ions, whereas the F3 sites between the Pb^{2+} layers are fully occupied. We recall that the simulations were initialized from a configuration in which only ideal fluorite F1, F2 and F3 sites were occupied. The Sn^{2+} ions have adopted the five co-ordinate square pyramidal arrangement depicted in figure 6(*b*). This is a remarkable finding for this simple ionic potential,

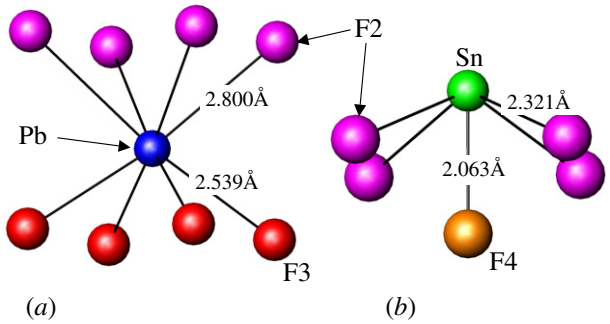

Figure 6. The anion environments surrounding (*a*) the Pb^{2+} and (*b*) the Sn^{2+} within α-$PbSnF_4$. Only single representative bond lengths are shown because all distances from the cations to equivalent anion sites are constrained by symmetry to be equal.

since this co-ordination structure is often seen as reflecting the stereochemical requirements of the lone-pair on the Sn^{2+} ion; we will discuss an alternative interpretation below.

The distribution of F^- ions within the Pb^{2+}–Sn^{2+} layers at 700 K (figure 5(*a*)) has not been constrained to adopt $P4/nmm$ symmetry but is, nevertheless, broadly in agreement with the locations of the F2 and F4 sites determined by the powder neutron diffraction studies of α-$PbSnF_4$ (figure 3). At temperatures immediately below the melting point of the simulations the F^- density becomes extremely disordered (see figure 5(*b*)). The evolution of the diffusion mechanism within the simulations of α-$PbSnF_4$ with increasing temperature will be discussed further in the following section.

5. Discussion

The structural model for α-$PbSnF_4$ determined by the powder neutron diffraction studies and illustrated in figure 3 contains the layered cation sequence PbPbSnSnPbPb$\cdots$ reported previously in this polymorph and other phases formed at ambient temperature by different synthesis methods [15, 17, 20–29]. However, the description of the anion distribution within α-$PbSnF_4$ is somewhat simpler than those presented previously and, at temperatures close to ambient, an excellent fit to the experimental diffraction data can be obtained using a model with only three fully occupied crystallographic sites. The use of neutron diffraction is key to the elucidation of this structure, since its increased sensitivity to the time-averaged distribution of the anions offers significant advantages over its x-ray counterpart, whilst the lack of a form factor provides data to lower d-spacings which is essential for extracting reliable information concerning the thermal vibrations. The use of anisotropic temperature factors appears to model the complex distribution of anion density within the Pb^{2+}–Sn^{2+} layers rather well. Undoubtedly, this description is an approximation to the real situation, which inevitably contains a degree of short-range order. However, as discussed in section 3.2, attempts to use more complex models involving additional sites with fractional occupancies did not provide statistically significant reductions in the goodness-of-fit χ^2 factor.

The anion co-ordination around the Pb^{2+} and Sn^{2+} cations is illustrated in figure 6. The eight Pb^{2+}–F^- contacts are formed by two sets of four within a slightly distorted cubic environment (figure 6(*a*)), with values spanning the single distance of 2.567 Å observed within the ideal cubic arrangement of β-PbF_2 [47]. The anion co-ordination surrounding the Sn^{2+} in α-$PbSnF_4$ is more irregular (figure 6(*b*)), with a single shorter contact along the

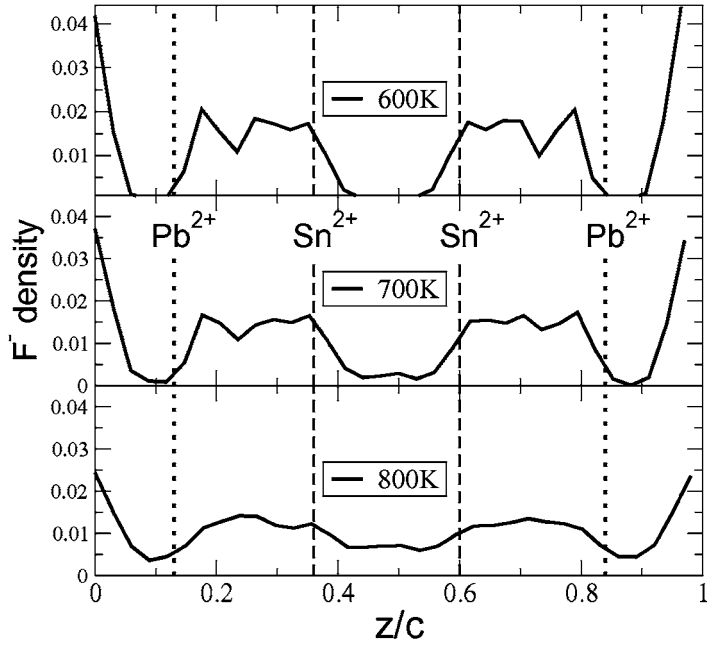

Figure 7. A one-dimensional view of the F^- ion density within the simulations of α-$PbSnF_4$ at temperatures of 600, 700 and 800 K. The F^- density is shown as a function of height through the unit cell. The vertical dashed lines in this figure denote the average positions of the Pb^{2+} and Sn^{2+} layers.

c-axis. As mentioned previously, this environment is traditionally interpreted in terms of a stereochemically active $5s^2$ lone-pair of the Sn^{2+}, with the pseudo-octahedral co-ordination SnF_5E and the lone-pair E pointing into the Sn^{2+}–Sn^{2+} interlayer space. Similar F^- environments around Sn^{2+} are observed in the α form of SnF_2 [45] and, in a more distorted manner, within β-SnF_2 [48]. The somewhat closer cation–anion contacts around the Sn^{2+} than the Pb^{2+} are also consistent with EXAFS investigations of α-$PbSnF_4$ [49]. As discussed in section 4.2, there is some discrepancy between the melting temperature of $PbSnF_4$ determined by experimental and simulation methods. However, of particular importance for this paper is the level of agreement between the experimental data and simulation results describing the cation environments. Taken together with the agreement on other key features, such as the unit cell volumes and the temperature dependence of the ionic conductivity, this provides confidence in the validity of the interionic potentials used for the simulations and justifies a deeper probing of their results.

A simplified one-dimensional view of the F^- ion density at temperatures of 600, 700 and 800 K is shown in figure 7, where the F^- density is shown as a function of height through the unit cell and the locations of the Pb^{2+} and Sn^{2+} layers are illustrated by the vertical dashed lines. Referring first to the lowest temperature (600 K), the sharp peaks in the F^- density at either side of the cell correspond to the ions on the well-ordered F3 sites, between the Pb^{2+}–Pb^{2+} layers. At this temperature, there are no F^- ions between the Sn^{2+}–Sn^{2+} layers. Between the Pb^{2+} and Sn^{2+} ions there is a sharp peak closest to the Pb^{2+} ions which corresponds to the F4 site in the experimentally determined crystal structure (figure 3), whereas the other broader feature represents the F2 site. As the temperature is raised, the overall structure remains the same, but the minima begin to fill in as a consequence of the ionic motion. By 800 K, where

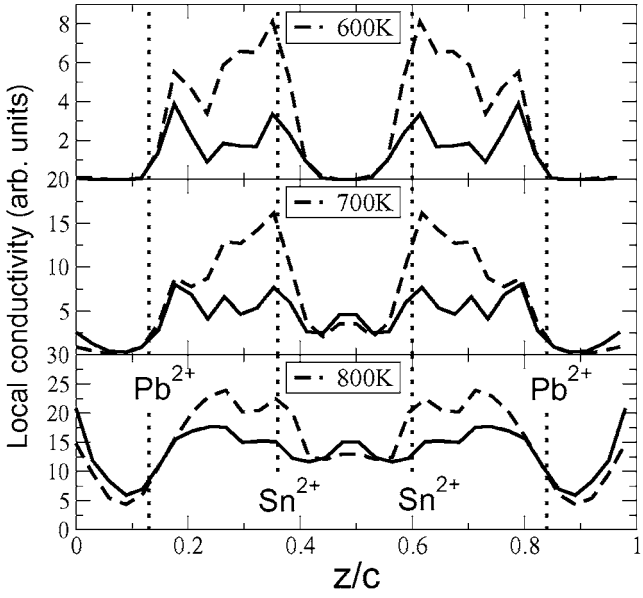

Figure 8. The local conductivities associated with F^- motion within the simulations of α-$PbSnF_4$ parallel to (solid curve) and perpendicular to (dashed curve) the c-direction of the unit cell at temperatures of 600, 700 and 800 K. The vertical dashed lines in this figure denote the average positions of the Pb^{2+} and Sn^{2+} layers.

the simulated system is close to melting, it would appear that there are a significant number of F^- ions in the Sn^{2+}–Sn^{2+} layers, and that the ions in F3 sites are beginning to exchange with those from other sites within the cell.

The same representation can be used to describe the nature of the ionic motion which contributes to the conductivity. In figure 8 we show a measure of the local conductivities associated with motion parallel to and perpendicular to the c-direction of the unit cell. These conductivities are obtained from the mean-squared displacements of an ion initially located at the position z parallel to and perpendicular to the z-direction. These are given by

$$\Delta_{\parallel}^2(z,t) = \langle |z_i(t) - z_i(0)|^2 \delta(z_i(0) - z) \rangle$$

and

$$\Delta_{\perp}^2(z,t) = \langle \tfrac{1}{2}\{|x_i(t) - x_i(0)|^2 + |y_i(t) - y_i(0)|^2\} \delta(z_i(0) - z) \rangle$$

in terms of the cell-frame co-ordinates of ion i and with $\langle \cdots \rangle$ meaning an average over all ions and initial times. The mobility is found from the difference between the displacements after two delay times t_1 and t_2, as if taking the gradient of the mean-squared displacement versus time in order to evaluate a diffusion coefficient. Using values for t_1 and t_2 of 2 and 8 ps means that the oscillatory motion of ions about their lattice sites does not contribute to this measure of the mobility. Finally, the mean mobility of an ion in the slab at z is multiplied by the number of ions in that slab to give a measure of the contribution of that slab to the overall conductivity. The upper panel of the figure shows that the ions in the F3 sites (between the Pb^{2+} layers) are immobile at 600 K; this implies that the conduction of the crystal is two dimensional, since any passage of ions through this region would have resulted in a finite value. The conductivity at this temperature is entirely due to the ions between the Pb^{2+} and Sn^{2+} layers, which is seen to be highly anisotropic. Mobile ions reside in both the F2 and F4 sites and they appear to

interconvert rapidly. As the temperature is raised to 700 K, the small number of ions between the Sn^{2+} layers (see figure 8) are seen to be highly mobile; note that the sense of anisotropy here is reversed, with the ions moving more rapidly along the *c*-direction, suggesting that the ions found here are in the process of passing between Sn^{2+} and Pb^{2+} layers. The ions in the F3 sites are now slightly mobile, with again more rapid motion along the *c*-direction. Within the Sn^{2+}–Pb^{2+} layers, the motion appears less anisotropic than at lower temperatures. By 800 K, ions are moving throughout the cell, and the motion is becoming quite isotropic. This trend is consistent with the behaviour of the real system, though the three-dimensional character of the ionic diffusion within the γ phase of $PbSnF_4$ (stable within a narrow temperature range immediately below the melting point [17, 20]) is associated with disorder of the two cation species to form a cubic phase (space group $Fm\bar{3}m$) which is, on average, isostructural with the fluorite-structured form of β-PbF_2.

Whilst initial *NPT* simulations of a cation-disordered γ phase resulted in a stable cubic structure, monitoring the ionic displacements in the subsequent *NVT* runs showed that this phase melted at a temperature of about 830 K, slightly below the α phase. This observation would suggest that the γ phase is slightly less stable than the α phase in the simulations, contrary to the experimental findings. Furthermore, the calculated conductivities for the γ phase were much lower than for the α phase and it would appear that the present potential is unable to recapture the F^- disorder within the γ-$PbSnF_4$ phase correctly. Nevertheless, the finding that an ionic potential, in which the Sn^{2+} ion is *a priori* spherical and which contains no explicit representation of the electronic structure, gives a five co-ordinate square planar co-ordination geometry for the Sn^{2+} ion at first sight seems to contradict the normal attribution of this geometry to the stereochemical requirements of the lone-pair. However, recall that the large polarizability of the Sn^{2+} ion arises from the ns^2 electronic configuration, and then when the ion is in the five-fold structure the negative end of the induced dipole will point away from the apical F^- into the space where the lone-pair would be expected to reside. The induction of a dipole can only lower the energy of a particular structure and it would appear that, for an ion as polarizable as Sn^{2+}, this effect lowers the energy of the five-fold structure sufficiently to stabilize it relative to the cubic one characteristic of the fluorite case, which is of such high symmetry that no dipole can be induced. Why then is the same structure not observed at the Pb^{2+} site, given that the dipole polarizability of Pb^{2+} is greater than that of Sn^{2+}? This must be due to the smaller size of the Sn^{2+} cation, which allows a closer approach of the F^- ion and hence a larger polarizing field.

6. Conclusions

The complementary use of impedance spectroscopy, powder neutron diffraction and computer simulation methods has provided a consistent picture of the anion diffusion mechanism within α-$PbSnF_4$ at temperatures close to ambient. The observed high ionic conductivity of this material is remarkable, since conduction involves only a fraction of the anions and is restricted to two-dimensional planes. This finding is contrary to the recent studies of Ahmad *et al* [24], in which ^{19}F NMR studies indicated that all anions contribute to the conduction process with $PbSnF_4$ at temperatures close to ambient. However, x-ray diffraction data presented in that work indicated an orthorhombic structure and they are not, therefore, directly comparable to the α form discussed here. A more instructive comparison is $BaSnF_4$, which is isostructural with α-$PbSnF_4$, except for the presence of a small fraction of F^- within the Sn^{2+}–Sn^{2+} layers [50]. ^{19}F and ^{119}Sn NMR studies of $BaSnF_4$ are interesting because its lower ionic conductivity means that the timescales of fluorine motion fall on the timescales probed by high-resolution NMR methods. These indicate that two anion sublattices are present: one comprising immobile

F^- within the Ba^{2+}–Ba^{2+} layers (F3 sites) and the other the remaining anions within the Ba^{2+}–Sn^{2+} and Sn^{2+}–Sn^{2+} layers which undergo rapid exchange with one another to generate essentially two-dimensional conduction [50, 51].

Despite its high ionic conductivity at temperatures close to ambient, the complex polymorphism and apparent irreproducibility of the properties of $PbSnF_4$ represent an obstacle to its commercial exploitation within solid state devices. It is hoped that these studies will motivate further investigations of this important material (both experimental and simulation), including studies of its behaviour with a disordered $Pb^{2+} + Sn^{2+}$ cation array, as observed at temperatures close to melting (γ-$PbSnF_4$ [17, 20]) or formed as a metastable phase at ambient temperature by ball milling [30]. In a wider sense, highly polarizable cations such as Bi^{3+}, Pb^{2+}, Sn^{2+} and Tl^+ are known to be common constituents of many highly conducting oxide and halide phases, and the extensive anion disorder has often been attributed to the presence of electron lone-pairs (for a recent review, see [3]). The development of interionic potentials based on *ab initio* calculations which can successfully reproduce the structure and ionic conducting properties of such cation species is a major advance in the use of computer simulation techniques to probe the diffusion mechanisms which characterize the high ionic conductivity of many superionic compounds.

Acknowledgments

One of the authors (PB) wishes to thank the Swedish Research Council. The authors are also grateful to D S Sivia and M Wilson for their assistance with the maximum entropy difference Fourier and computer simulation techniques, respectively.

References

[1] Chandra S 1981 *Superionic Solids: Principles and Applications* (Amsterdam: North-Holland)
[2] Hayes W 1978 *Contemp. Phys.* **19** 469–86
[3] Hull S 2004 *Rep. Prog. Phys.* **67** 1233–314
[4] Hutchings M T, Clausen K, Dickens M H, Hayes W, Kjems J K, Schnabel P G and Smith C 1984 *J. Phys. C: Solid State Phys.* **17** 3903–40
[5] Goff J P, Hayes W, Hull S and Hutchings M T 1991 *J. Phys.: Condens. Matter* **3** 3677–87
[6] Schröter W and Nölting J 1980 *J. Physique Coll.* **41** C6 20–3
[7] Castiglione M J, Wilson M and Madden P A 1999 *J. Phys.: Condens. Matter* **11** 9009–24
[8] Kennedy J H and Miles R C 1976 *J. Electrochem. Soc.* **123** 47–51
[9] Liang C C and Joshi A V 1975 *J. Electrochem. Soc.* **122** 466–70
[10] Yoshikado S, Ito Y and Réau J M 2002 *Solid State Ion.* **154/155** 503–9
[11] Lucat C, Rhandour A, Cot L and Reau J M 1979 *Solid State Commun.* **32** 167–9
[12] Lagassie P, Grannec J and Reau J M 1986 *Solid State Ion.* **21** 343–8
[13] Ito Y, Mukoyama T, Ashio K, Yamamoto K, Suga Y, Yoshikado S, Julian C and Tanaka T 1998 *Solid State Ion.* **106** 291–9
[14] Vilminot S, Perez G, Granier W and Cot L 1981 *Solid State Ion.* **2** 91–4
[15] Vilminot S, Perez G, Granier W and Cot L 1981 *Solid State Ion.* **2** 87–90
[16] Donaldson J D and Senior B J 1967 *J. Chem. Soc.* A 18221–5
[17] Réau J-M, Lucat C, Portier J, Hagenmuller P, Cot L and Vilminot S 1978 *Mater. Res. Bull.* **13** 877–82
[18] Tovar L L G, Connor P A, Belliard F, Torres-Martínez L M and Irvine J T S 2001 *J. Power Sources* **97/98** 258–61
[19] Eguchi T, Suda S, Amasaki H, Kuwano J and Saito Y 1999 *Solid State Ion.* **121** 235–43
[20] Pannetier J, Denes G and Lucas J 1979 *Mater. Res. Bull.* **14** 627–31
[21] Pérez G, Vilminot S, Granier W and Cot L 1980 *Mater. Res. Bull.* **15** 587–93
[22] Chernov S V, Moskvin A L and Murin I V 1991 *Solid State Ion.* **47** 71–3
[23] Dénès G, Milova G, Madamba M C and Perfiliev M 1996 *Solid State Ion.* **86–88** 77–82
[24] Ahmad M M, Yamada K and Okuda T 2002 *J. Phys.: Condens. Matter* **14** 7233–44

[25] Denes G, Pannetier J and Lucas J 1975 *C. R. Acad Sci.* **280** 831–4
[26] Kanno R, Nakamura S, Ohno K and Kawamoto Y 1991 *Mater. Res. Bull.* **26** 1111–7
[27] Ito Y, Mukoyama T, Funatomi H, Yoshikado S and Tanaka T 1994 *Solid State Ion.* **67** 301–5
[28] Kanno R, Ohno K, Izumi H, Kawamoto Y, Kamiyama T, Asano H and Izumi F 1994 *Solid State Ion.* **70/71** 253–8
[29] Ito Y, Mukoyama T and Yoshikado S 1995 *Solid State Ion.* **80** 317–20
[30] Collin A, Dénès G, le Roux D, Madamba M C, Parris J M and Salaün A 1999 *Int. J. Inorg. Mater.* **1** 289–301
[31] Gardner N J G, Hull S, Keen D A and Berastegui P 1998 *Rutherford Appleton Laboratory Internal Report* RAL-TR-1998-032
[32] Hull S, Smith R I, David W I F, Hannon A C, Mayers J and Cywinski R 1992 *Physica* B **180/181** 1000–2
[33] Sivia D S and David W I F 2001 *J. Phys. Chem. Solids* **62** 2119–27
[34] Hull S, Keen D A, Sivia D S and Berastegui P 2002 *J. Solid State Chem.* **165** 363–71
[35] Hull S, Keen D A, Sivia D S, Madden P A and Wilson M 2002 *J. Phys.: Condens. Matter* **14** L9–17
[36] David W I F, Ibberson R M and Matthewman J C 1992 *Rutherford Appleton Laboratory Internal Report* RAL-92-032
[37] Brown P J and Matthewman J C 1987 *Rutherford Appleton Laboratory Internal Report* RAL-87-010
[38] Wilson A J C (ed) 1995 *International Tables for Crystallography* vol C (Dordrecht: Kluwer)
[39] Castiglione M J, Wilson M, Madden P A and Grey C P 2001 *J. Phys.: Condens. Matter* **13** 51–66
[40] Castiglione M J and Madden P A 2001 *J. Phys.: Condens. Matter* **13** 9963–83
[41] Pyper N C 1986 *Phil. Trans. R. Soc.* A **320** 107–58
[42] Fowler P W and Pyper N C 1985 *Proc. R. Soc.* A **398** 377–93
[43] Wilson M and Madden P A 1993 *J. Phys.: Condens. Matter* **5** 2687–706
[44] Tang K T and Toennies J P 1984 *J. Chem. Phys.* **80** 3726–41
[45] Denes G, Pannetier J, Lucas J and Le Marouille J Y 1979 *J. Solid State Chem.* **30** 335–43
[46] Martyna G J, Tobias D J and Klein M L 1994 *J. Chem. Phys.* **101** 4177–89
[47] Wyckoff R W G 1982 *Crystal Structures* (Melbourne, FL: Krieger)
[48] Denes G, Pannetier J and Lucas J 1980 *J. Solid State Chem.* **33** 1–11
[49] Denes G, Yu Y H, Tyliszczak T and Hitchcock A P 1991 *J. Solid State Chem.* **91** 1–15
[50] Chaudhuri S, Wang F and Grey C P 2002 *J. Am. Chem. Soc.* **124** 11746–57
[51] Durand-Le Floch M, Pannetier J and Denes G 1986 *Phys. Rev.* B **33** 632–4